Determinants restricting ACE2 recognition of MERS-related coronaviruses in bats

Chengbao Ma[1*],Qing Xiong[1,*], Mengxue Gu[1], Chunli Wang[1], Lulu Shi[1], Chen Liu[1], Junyu Si[1], Fei Tong[1], Peng Liu[1], Meiling Huang[1], Huan Yan[1] ✉

[1]State Key Laboratory of Virology, Institute for Vaccine Research and Modern Virology Research Center, College of Life Sciences, Wuhan University, Wuhan, Hubei, China.

[*]These authors contributed equally.

✉e-mail: huanyan@whu.edu.cn

Abstract

Phylogenetically distant coronaviruses have evolved to employ ACE2 as their common receptors, including NL63 and many Severe acute respiratory syndrome (SARS) coronavirus-related viruses[1]. Recently, we found two Middle East respiratory syndrome coronaviruses (MERS-CoV)-related bat coronaviruses, NeoCoV and PDF-2180, also use Angiotensin-converting enzyme 2(ACE2) but not MERS-CoV receptor dipeptidyl peptidase 4 (DPP4) for entry[2]. Receptor binding domain (RBD)-binding and pseudovirus entry assays based on a wide range of bat ACE2 orthologs revealed that the two viruses strongly prefer ACE2 from *Yangochiropteran* bats as compared with *Yinpterochiropteran* bats, which is not observed in NL63 and SARS-CoV-2. Genetic and structural analyses of the virus-receptor interactions of 50 bat ACE2 orthologs pointed to four crucial host range determinants in two viral binding loops on ACE2. Subsequent functional verifications via mutagenesis on representative ACE2 orthologs confirmed the importance of these determinants on human and bat cells. Remarkably, NeoCoV-T510F, a mutation previously shown to acquire human ACE2 recognition, displayed an expanded potential host range covering most tested bat ACE2, probably due to its reinforced interaction with an evolutionary conserved hydrophobic pocket. Our results elucidated the molecular mechanisms for the species-specific ACE2 usage of MERS-related viruses, offering basic information for assessing the zoonotic risk of these ACE2 utilizing merbecoviruses.

Keywords: Bat coronavirus, MERS-CoV, NeoCoV, ACE2, bats, host range determinants

Introduction

Emerging coronaviruses associated with several outbreaks in the 21st century impose severe threats to human health[3-6]. Being the most important reservoirs of at least hundreds of α- and β-coronaviruses (CoVs), bats are the crucial hosts of evolutional ancestors and relatives of many high-risk human CoVs, including SARS-CoV, SARS-CoV-2, and MERS-CoV [7-11]. Although the origin of highly pathogenic MERS-CoV remains elusive, hypotheses have been proposed that MERS-CoV may arise from the recombination and evolution of MERS-related bat coronaviruses[12-14]. NeoCoV and PDF-2180 are MERS-related viruses (merbecoviruses subgenus) sampled in vesper bats harbors in South Africa and Southwest Uganda, respectively [15,16]. NeoCoV represents the yet-identified closest relative of MERS-CoV in bats with ~85% whole genome nucleotide similarity[17]. However, its RBD sequence and structure are very different from MERS-CoV[2,15].

Several merbecoviruses use their host's DPP4 as entry receptors, such as MERS-CoV, bat CoV HKU4, and HKU25, whereas the receptors for many other merbecoviruses remain elusive[15,18-20]. Recently, we reported that NeoCoV and PDF-2180 unexpectedly engage bat ACE2 as their receptors [2]. Cryo-electron microscopy (Cryo-EM) analysis of NeoCoV or PDF-2180 RBD in complex with a bat ACE2 from *Pipistrellus pipistrellus* (Ppip) revealed a relatively small and flat ACE2 binding surface characterized by an N-glycosylation mediated protein-glycan interaction, a mode distinct from other ACE2 utilizing viruses.

Receptor recognition is usually species-specific and determines the cross-species transmission potential of CoVs. For example, SARS-CoV and SARS-CoV-2 exhibited varying efficiency to use ACE2 orthologs from different bat species[21]. NeoCoV and PDF-2180 highly preferred ACE2 orthologs from *Yangochiropteran* bats (Yang-bats) for entry[2]. Comparatively, human ACE2 (hACE2) is not efficiently recognized by these viruses, whereas adaptive spike mutations like T510F on receptor binding motif (RBM) enhanced hACE2 binding affinity. Interestingly, most tested ACE2 orthologs from Yin-bats were even more defective in supporting viral binding and entry of the two viruses than wild-type (WT) hACE2, indicative of specific host range determinants among bat species[2].

Here, we extensively explored the determinants restricting ACE2 orthologs from Yin-bats of supporting NeoCoV and PDF-2180 entry. Four species-specific sites within the binding interface were identified and confirmed as potential host range determinants, including two N-glycosylation sites.

Results

Bat-specific receptor usage of ACE2 utilizing viruses

We previously showed that ACE2 orthologs from most tested (14/15) Yin-bats and very few (2/30) Yang-bats (Nlep and Nhum) were deficient in supporting NeoCoV and PDF-2180 RBD binding and pseudovirus entry[2]. In this study, we re-examined the receptor function of 18 Yin-Bat's ACE2 for NeoCoV, including three (Rcor, Raff, and Rmal) we subsequently found capable of supporting NeoCoV and PDF-2180 RBD entry. ACE2 orthologs from four Yang-bats (Nlep, Ppip, Lbor, and Nhum) and hACE2 were also included. Immunofluorescence assay detecting the C-terminal fused 3×Flag tags indicated these receptors were expressed at a similar level (**Extended data figure 1)**. The results of the NeoCoV RBD binding and pseudovirus entry assays were generally consistent and further confirmed our previous observation that most, but not all, Yin-bats' ACE2 are deficient in supporting NeoCoV entry (**Fig.1a-b**). We next investigated whether the species-specific bat ACE2 preference can be observed in other representative ACE2 utilizing viruses: PDF-2180, SARS-CoV-2, and NL63. The receptor binding modes of the four viruses are shown in **Fig.1c**, highlighted with distinct RBD binding footprints. NeoCoV and PDF-2180 RBD binding and pseudovirus entry exhibited very similar profiles among the 22 tested bat ACE2 orthologs and are very different from those of SARS-CoV-2 and NL63, consistent with the distinct receptor binding modes of these viruses **(Fig.1d and extended data figure 1 and 2)**. SARS-CoV-2, which is supposed to share common ancestors infecting Yin-bats (*Rhinolophus malayanus*, Rmal)[9], can efficiently use 12 ACE2 from Yin-bats. Although the close relatives of NL63 were sampled in *Yang*-bat (*Perimyotis subflavus*)[22], efficient binding and entry of NL63 can also be supported by most (14/18) tested Yin-bats' ACE2. These data indicate that the species-specificity is not strictly correlated with the phylogeny, and additional determinants are affecting the functionality of ACE2 from various bats in mediating NeoCoV and PDF-2180 infection.

90

91 **Identification of potential host range determinants restricting NeoCoV/PDF-2180 recognition**

92 We next sought to identify the host range determinants by combining genetic, structural, and
93 functional analyses focusing on sequences of the two critical RBD interacting loops, both of which
94 contain an important glycosylation site **(Fig.2a)**. We first conducted multiple sequence alignment
95 and conservation analyses based on 50 bat ACE2 sequences (from 19 Yin- and 31 Yang-bats), which
96 are separated into two groups by their ability to support NeoCoV entry **(Fig.2b and Extended data**
97 **3 and 4)**. These results highlighted four candidate sites (from A-D) with contrasting residue
98 frequency across the two groups **(Fig.2c)**. According to the presence of deficient/sub-optional
99 residues, we classified the ACE2 orthologs deficient in viral receptor functions into several
100 corresponding defect types **(Fig.2d).** For example, Raeg ACE2 was designated defect type ABCD as
101 it carries deficient residues on all four predicted sites. We next analyzed the impact of the
102 deficient/sub-optimal ACE2 residues on viral RBD recognition via structural modeling based on the
103 Ppip ACE2-NeoCoV-RBD complex **(Fig.2d)**. Glycosylations sites (N-X-T/S) in A and C involved in
104 in the glycan-protein interactions are missing in several Yin-bats' ACE2. Site A glycosylation (N54
105 glycosylation) seems more important than site C glycosylation (N330-glycosylation) as it mediated a
106 protein-glycan interaction required for stabilizing RBD in Region 1. In contrast, site C glycosylation
107 only partially contributes to the extensive interactions in region 2 via forming hydrogen bonds with
108 two RBM glycines of NeoCoV but not PDF-2180. Residues in sites B and D of Yin-bats' ACE2
109 either abolish the polar contacts (e.g., two salt bridges formed by residues E305 and D338,
110 respectively) or introduce steric clashes (e.g., E305K) that reduce the binding affinity. It is worth
111 mentioning that site D, especially the D338, is a critical host range determinant restricting hACE2
112 from efficiently supporting the binding and entry of the two viruses[2].

113

114 **Functional verification of host range determinants of NeoCoV/PDF2180 in bat ACE2**

115 To explore the role of candidate determinants, we picked representative ACE2 orthologs of
116 specific defect types for gain-of-function tests. Specifically, a series of point or swap mutagenesis
117 based on ACE2 orthologs from Rsin (type A), Rfer and Rpea (type B), Hgal (type BC), Nlep (type
118 BCD), and Raeg (type ABCD) were conducted to test their positive effects in supporting
119 NeoCoV/PDF2180 RBD binding and entry. Rsin-N55T (type A) with an amended N53 glycosylation

site (corresponding to N54 in Ppip ACE2) showed remarkable improvements in supporting RBD binding and viral entry **(Fig.3a-b and Extended data figure 5)**. Rfer-K305E (type B) and Rpea-N305E (type B*), with introduced salt bridges, also exhibited significantly improved receptor functions (**Fig.3c-d and Extended data figure 5 and 6**). Efficient binding and entry supported by bat ACE2 mutants from Hgal (type BC) and Nlep (type BCD) can be observed after corresponding residues are substituted with Ppip ACE2 counterparts **(Extended data figure 6)**. Particularity, a gradual gain of receptor function of Raeg ACE2 (type ABCD) can be observed by stepwise increasing substitutions in sites A, AB, ABC, and ABCD, respectively **(Fig.3e-g)**. Similar gain-of-function of Rsin-N55T and Raeg ACE2-ABCD was also confirmed on a Bat cell line Tb 1 Lu **(Extended data figure 7)**. We further evaluated the binding affinity between viral RBDs proteins and representative WT and mutant ACE2 by Flow cytometry and Bio-layer interferometry (BLI) assays **(Fig.3h-i)**. As expected, the binding affinities between WT Raeg/Rsin ACE2 and NeoCoV/PDF-2180 RBDs were below the detection limit, but the related mutations significantly improved their RBD binding affinities, with apparent binding affinities ($K_{D,\ app}$) ranging from 2.04×10^{-8} to 6.94×10^{-10} **(Fig.3i)**. Together, these results demonstrated that all the tested bat ACE2 orthologs with poor receptor function for NeoCoV and PDF-2180 could be primarily attributed to the deficient/sub-optional residues in the four predicted host range determinants.

RBM mutations broaden the potential host range of NeoCoV

We previously reported that specific mutations of NeoCoV and PDF-2180 RBM confer hACE2 recognition[2]. For NeoCoV, a T510F mutation increasing RBM local hydrophobicity enhanced its interaction with a hydrophobic pocket of ACE2 (**Fig.4a**). Sequence analysis of the 50 bat ACE2 indicated residues constituting this hydrophobic pocket are highly conserved among bat species (**Fig.4b**). Thus, we hypothesized that mutations such as T510F could expand the potential host range by recognizing Yin-bats via increasing hydrophobic interactions with this pocket. As expected, NeoCoV-T510F efficiently binds with most tested ACE2 orthologs and can achieve robust entry by these receptors, except for Rsin and Raeg ACE2 without the critical N53 glycosylations (**Fig.4c-d**). Further experiments demonstrated that Rsin ACE2-N55T and Raeg ACE2-I55T with functional N53 glycosylation sites achieved efficient NeoCoV-T510F entry (**Fig.4e-f**). These results indicate that NeoCoV, PDF-2180, or related viruses may efficiently infect Yin-bats through antigenic

150 drifts on RBM and further highlight the importance of N53 glycan in species-specific ACE2
151 recognition.
152
153
154 **Discussion**
155 The order Chiroptera comprises more than 1,400 bat species with remarkable diversity and wide
156 geographic distribution[23]. These bats are considered natural reservoirs of hundreds of known α- and
157 β-CoVs and important hosts for viral evolution[8]. Critical residues on viral receptors responsible for
158 spike protein binding exhibit accelerated evolution in bats[24,25], resulting in species-specificity in
159 supporting coronavirus binding and entry, which has been reported in SARS-CoV, SARS-CoV-2,
160 and MERS-CoV[21,26]. To date, coronaviruses of three different subgenera have evolved to engage
161 ACE2 for cellular entry, including NL63 (Setracovirus subgenus, α-CoV), many SARS-related CoVs
162 (Sarbecovirus subgenus, β-CoV), and two recently reported MERS-related CoVs (Merbecovirus
163 subgenus, β-CoV) in this study [1,2]. The distinct viral RBD structure and ACE2 binding footprints
164 suggest convergent evolutionary histories of receptor adaptation of these viruses[2].
165 In this study, we demonstrated that NeoCoV and PDF-2180 prefer ACE2 orthologs from
166 Yang-bats but not from most Yin-bats, while NL63 and SARS-CoV-2 displayed very different usage
167 profiles. This receptor preference is in line with the observation that most Merbecoviruses were
168 sampled in bats belonging to the family *Vespertilionidae* (vesper bats), the largest family of
169 *Yangochiroptera* (**Extended data figure 3**), including the hosts of NeoCoV and PDF-2180[8].
170 Comparatively, most sarbecoviruses were identified in Yin-bats, particularly *Rhinolophine* or
171 *Hipposideros*[8,27]. The differences in host preference likely limited the opportunities for cross-lineage
172 recombination of these high-risk viruses.
173 We here revealed that the receptor preference is determined by specific sequences in the viral
174 binding interface of ACE2 orthologs. Interestingly, glycan-protein interactions play a vital role in
175 species-specific ACE2 recognition of Merbecoviruses, especially the crucial interaction mediated by
176 N54-(or N53 in Rsin and Raeg) glycosylation. Similar glycan-protein interaction in receptor
177 engagement has also been reported in other coronaviruses, including SARS-CoV-2 and
178 human-infecting CCoV-HuPn-2018[28,29]. It could be interesting to investigate their contribution to
179 host range determination in other coronaviruses. The other three determinants were close to the N329

180 (or N330 in some species) glycosylation. Since only some Yang-bats carry glycosylation at this site,
181 its contribution to binding affinity and species specificity is less important than the N53
182 glycosylation, probably due to the compensation of nearby protein-protein interactions. Other than
183 the two glycosylation, site B and D determinants represent two critical sites that participated in
184 protein-protein interactions required for effective receptor recognition. Both sites of most Yang-bats'
185 ACE2 form salt bridges with viral RBMs. Although site D has been demonstrated to restrict hACE2
186 recognition, the interaction mediated by site B (residue 305) seems to play a more significant role in
187 host range determinants in bats. Most ACE2 from Yin-bats lack an E305 in site B, which forms a salt
188 bridge with the RBM of the viruses (e.g., K512 in NeoCoV) in most Yang-bat. N305 in several
189 Yin-bats forms sub-optional hydrogen bonds with the viruses, while K305 seems unable to interact
190 with the viruses and may even result in steric hindrance.

191 Receptor recognition is a primary barrier to cross-species transmission of coronaviruses, while
192 adaptive antigenic drift could break this barrier and lead to spillover in other species[30]. Here we show
193 that the T510F mutation in the NeoCoV spike, increasing binding affinity via interacting with a
194 conserved hydrophobic pocket, broadens the potential host range. Our results indicate that NeoCoV
195 and related viruses hold the potential to break the current host range barrier of ACE2 incompatibility
196 through antigenic drift or recombination. Moreover, these ACE2-using merbecoviruses may also
197 have more competent relatives in the wild that are not yet on our radar.

198 Taken together, our study elucidated the species-specific ACE2 recognizing mechanism of
199 MERS-related viruses and identified several critical residues on the binding interface for host range
200 determination. Our study adds knowledge to the long-neglected and potentially high-risk
201 coronaviruses, which is crucial for virus surveillance in various species to prepare for future
202 outbreaks.

203

204 **Methods**

205 **Cell lines**

206 HEK293T (CRL-3216) and the bat epithelial cell line Tb 1 Lu (CCL-88) were purchased from
207 American Type Culture Collection (ATCC). Cells were maintained by Dulbecco's Modified Eagle
208 Medium (DMEM, Monad, China) with 1% PS (Penicillin/Streptomycin) and 10% Foetal Bovine
209 Serum. An I1-Hybridoma (CRL-2700) cell line secreting a neutralizing mouse monoclonal antibody

210 targeting the VSV glycoprotein (VSVG) was cultured in Minimum Essential Medium(MEM) with
211 Earles's balances salts and 2.0 mM of L-glutamine (Gibico) and 10% FBS. All the cells were
212 cultured at 37°C with 5% CO_2 with regular passage every 2-3 days.
213
214 **Plasmids**
215 Plasmids expressing WT or mutated bats ACE2 orthologs were generated by inserting human
216 codon-optimized sequences with/without specific mutations into a lentiviral transfer vector
217 (pLVX-EF1a-Puro, Genewiz) with C-terminus 3×Flag (DYKDHD-G-DYKDHD-I-DYKDDDDK).
218 Human codon-optimized the spike sequences of NeoCoV (AGY29650.2), PDF-2180
219 (YP_009361857.1), SARS-CoV-2 (D614G) (YP_009724390.1), and NL63(APF29071.1) were
220 cloned into the PCAGGS vector with C terminal deletions (13-15 aa) to improve the assembly
221 efficiency. The plasmids expressing the recombinant CoVs RBD-hFc fusion proteins were
222 constructed by inserting NeoCoV RBD (380-585), PDF-2180 RBD (381-586), SARS-CoV-2 RBD
223 (331-524) and NL63 RBD (481-616) coding sequences into the pCAGGS vector containing an
224 N-terminal CD5 signal peptide (MPMGSLQPLATLYLLGMLVASVL) and a C-terminal hFc tag for
225 purification and detection. The expression plasmids of bats ACE2 ectodomain proteins were
226 generated by inserting WT or mutated sequences of Rousettus_aegyptiacus (18-740aa),
227 Rhinolophus_sinicus (18-740aa), and Pipistrellus_kuhlii (20-738 aa) into the pCAGGS vector with
228 an N-terminal CD5 signal peptide and a C-terminal twin-strep-3×Flag tag
229 (WSHPQFEKGGGSGGGSGGSAWSHPQFEKGGGRSDYKDHDGDYKDHDIDYKDDDDK).
230
231 **Bioinformatic and structural analysis**
232 Sequence alignments of different bats ACE2 were performed either by the MUSCLE algorithm by
233 MEGA-X (version 10.1.8) or ClustalW (https://www.genome.jp/tools-bin/clustalw) software. The
234 residue usage frequency (sequence logo) and mean hydrophobicity of 50 ACE2 sequences were
235 generated by the Geneious Prime software. Phylogenetic trees were produced using the maximal
236 likelihood method in MEGA-X (1000 Bootstraps) and polished with iTOL(v6) (https://itol.embl.de/)
237 [31]. The structural were shown by ChimeraX based on SARS-CoV-2 RBD & human ACE2(PDB:
238 6M0J), NL63 RBD & human ACE2(PDB: 3KBH), NeoCoV RBD & Ppip ACE2(PDB: 7WPO) and
239 PDF-2180 RBD & Ppip ACE2(PDB: 7WPZ). RBD binding footprints and interaction details were

240 analyzed and demonstrated using the UCSF ChimeraX[32]. Structural representatives of NeoCoV RBD
241 interacting with WT or mutated Ppip ACE2 were analyzed using the UCSF Chimera X. The colored
242 sequence conservation of 50 bats ACE2 was demonstrated by the UCSF ChimeraX based on
243 multi-sequence alignments data generated by MEGA-X.
244
245 **Protein expression and purification**
246 HEK293T transfected with different protein-expressing plasmids through the GeneTwin reagent
247 (Biomed, TG101-01). At 4-6 hours post-transfection, the medium of the transfected cells was
248 replenished with the SMM 293-TII Expression Medium (Sino Biological, M293TII), and the
249 protein-containing supernatant was harvested every three days 2-3 times. Recombinant RBD-hFc
250 proteins were captured by Pierce Protein A/G Plus Agarose (Thermo Scientific, 20424), washed by
251 wash buffer (100 mM Tris/HCl, pH 8.0, 150 mM NaCl, 1mM EDTA), eluted with pH 3.0 Glycine
252 buffer (100 mM in H2O), and then immediately balanced by 1/10 volume of UltraPure 1M Tris-HCI,
253 pH 8.0 (15568025, Thermo Scientific). Proteins with twin-strep tag were captured by Strep-Tactin
254 XT 4Flow high-capacity resin (IBA, 2-5030-002), washed by wash buffer, and then eluted by buffer
255 BXT (100 mM Tris/HCl, pH 8.0, 150 mM NaCl, 1mM EDTA, 50 mM biotin). The eluted proteins
256 were concentrated by Ultrafiltration tubes and buffer changed with PBS and stored at -80°C. Protein
257 concentrations were determined by the Omni-Easy Instant BCA Protein Assay Kit (Epizyme,
258 ZJ102).
259
260 **Coronavirus RBD-hFc live-cell binding assays**
261 Different coronavirus RBD-hFc recombinant proteins were diluted in DMEM at indicated
262 concentrations and incubated with live cells 36 hours post-transfection of different bat ACE2 for 30
263 mins at 37°C. After binding, cells were washed once by Hanks' Balanced Salt Solution (HBSS) and
264 then incubated with 2 μg/mL of Alexa Fluor 488-conjugated goat anti-human IgG (Thermo Fisher
265 Scientific; A11013) diluted in PBS/1% BSA for 1 hour at 37°C. Next, cells were washed once by
266 HBSS and then incubated with Hoechst 33342 (1:10,000 dilution in HBSS) for nucleus staining for
267 30mins at 37°C. Images were captured by a fluorescence microscope (MI52-N). The relative
268 fluorescence of the stained cells were determined by a Varioskan LUX Multi-well Luminometer
269 (Thermo Scientific). For flow cytometry analysis, the stained cells were detached by 5 mM of

270 EDTA/PBS and analyzed with a CytoFLEX Flow Cytometer (Beckman). 10,000 events in a gated
271 live cell population (based on SSC/FSC) were analyzed for all samples. HEK293T cells without
272 receptor expression were used as negative controls.
273
274 **Biolayer interferometry (BLI) binding assays**
275 BLI assays were performed on the Octet RED96 instrument (Molecular Devices) under the
276 manufacturers' instructions. In general, RBD-hFc recombinant proteins (20 μg/mL) were
277 immobilized on the Protein A (ProA) biosensors (ForteBio, 18-5010) and incubated with 2-fold
278 serial diluted bat ACE2-ectodomain proteins starting from 500nM in the kinetic buffer (PBST). The
279 background was set with a kinetic buffer without the ACE2-ectodomain proteins. The kinetic
280 parameters and binding affinities between the RBD-hFc and different bat ACE2 were analyzed by
281 Octet Data Analysis software 12.2.0.20 through curve-fitting kinetic or steady-state analysis.
282
283 **Pseudovirus production and titration**
284 VSV-dG-based pseudoviruses carrying CoVs spike proteins were produced based on a modified
285 protocol as previously described[33]. In general, HEK293T cells were transfected with CoVs spike
286 protein expression plasmids. At 24 hours post-transfection, cells were transduced with 1.5×10^6
287 $TCID_{50}$ VSV-G glycoprotein-deficient VSV expressing GFP and firefly luciferase
288 (VSV-dG-GFP-fLuc) diluted in DMEM with 8 μg/mL polybrene for 4-6 hours at 37 °C. After three
289 times of PBS wash, the culture medium was replenished with DMEM+10% FBS or SMM 293-TII
290 containing VSV neutralizing antibody (from I1-mouse hybridoma). Twenty-four hours later, the
291 virus-containing supernatant was clarified through centrifugation at 4,000 rpm for 5 mins at 4°C and
292 then stored at -80°C. $TCID_{50}$ of pseudotyped viruses were determined based on a three-fold
293 serial-dilution based infection assays on HEK293T-bat40ACE2 cells for NeoCoV and PDF-2180 S
294 pseudotypes, and 293T-hACE2 for NL63 and SARS-CoV-2 S pseudotypes. $TCID_{50}$ were calculated
295 according to the Reed-Muench method[34,35].
296
297 **Pseudovirus entry assay**
298 Pseudovirus entry assays were conducted on HEK293T or Tb 1 Lu cells transiently expressing WT
299 or mutant ACE2 orthologs at 36 hours post-transfection. In general, $3x10^4$ trypsinized cells were

300 incubated with pseudovirus (1.5×10^5 $TCID_{50}$/100μL) in a 96-well plate to allow attachment and viral
301 entry. TPCK-trypsin (Sigma-Aldrich, T8802) treatment was conducted before NeoCoV and
302 PDF-2180 pseudovirus entry assay. In this case, pseudovirus produced in FBS-free SMM-293-TII
303 medium were incubated with 100 μg/mL TPCK-treated trypsin for 10mins at room temperature,
304 followed by neutralization with 100 μg/mL soybean trypsin inhibitor (Sigma-Aldrich, T6414). The
305 intracellular luciferase activity was measured by Bright-Glo Luciferase Assay Kit (Promega, E2620)
306 and detected with a GloMax 20/20 Luminometer (Promega) at 18 hours post-infection. GFP intensity
307 were analyzed by a fluorescence microscope (Mshot, MI52-N).
308
309 **Western-Blot**
310 For Western Blot analysis, cells were lysed with 1% TritonX/PBS+1mM PMSF(Beyotime, ST506)
311 for 10 mins at 4°C, then clarified through centrifugation of 12000 rpm for 5 mins at 4°C. The
312 clarified cell lysate was mixed with the 1/5 volume of 5×SDS loading buffer and incubated at 98°C
313 for 10 mins. After gel electrophoresis and membrane transfer, the PVDF-membrane blots were
314 blocked with 5% skimmed milk in PBST for 2 hours at room temperature and then incubated
315 1μg/mL anti-Flag mAb (Sigma, F1804) or anti-glyceraldehyde-3-phosphate dehydrogenase
316 (GAPDH) (AntGene, ANT011) mAb diluted in PBST containing 1% milk overnight at 4°C. After
317 three times washing with PBST, the blots were incubated with Horseradish peroxidase
318 (HRP)-conjugated secondary antibody AffiniPure Goat Anti-Mouse IgG (H+L) (Jackson Immuno
319 Research, 115-035-003) in 1% skim milk in PBST and incubated for one hour at room temperature.
320 The blots were then washed three times by PBST and then visualized using an Omni-ECL Femto
321 Light Chemiluminescence Kit (EpiZyme, SQ201) by a ChemiDoc MP Imaging System (Bio-Rad).
322
323 **Immunofluorescence assay**
324 Immunofluorescence assays were conducted to verify the expression levels of ACE2 with C-terminal
325 fused 3×Flag. In general, the transfected cells were incubated with 100% methanol for 10 mins at
326 room temperature for fixation and permeabilization. Cells were then incubated with a mouse
327 antibody M2 (Sigma-Aldrich, F1804) diluted in PBS/1%BSA for one hour at 37°C, followed by
328 extensive wash and the incubation of secondary antibody of Alexa Fluor 594-conjugated goat
329 anti-mouse IgG (Thermo Fisher Scientific, A32742) diluted in 1% BSA/PBS for one hour at 37°C.

Before visualization, the nucleus was stained blue with Hoechst 33342 reagent (1:5,000 dilution in PBS). Images were captured and merged with a fluorescence microscope (Mshot, MI52-N).

Statistical Analysis

Most experiments were conducted 2-3 times with 3 or 4 biological repeats. Representative results were shown. Data were presented by MEAN±SD or MEAN±SEM as indicated in the figure legends. Unpaired two-tailed t-tests were conducted for all statistical analyses using GraphPad Prism 8. $P<0.05$ was considered significant. * $p<0.05$, ** $p<0.01$, *** $p<0.005$, and **** $p<0.001$.

Acknowledgements

Huan Yan was supported by China NSFC projects (32270164, 32070160) and Special Fund for COVID-19 Research of Wuhan University. We thank Beijing Taikang Yicai Foundation for their support to this work.

Author contributions

H.Y. and C.B.M. conceived and designed the study. C.B.M., Q.X. and H.Y. performed the experiments and analyzed the data. H.Y., C.B.M. and Q.X. interpreted the results. H.Y. and C.B.M. wrote the manuscript. H.Y. C.B.M. and Q.X revised the manuscript. M.X.G., C.L.W., L.L.S., C.L., J.Y.S., F.T., P.L.and M.L.H. commented on the manuscript.

Competing interests

The authors declare no competing interests.

Data availability

All data and information supporting the findings of this study are available with the paper and its supplementary information files.

Additional Information:

Correspondence and requests for materials should be addressed to H.Y. (huanyan@whu.edu.cn)

Figure legends

361

362 **Figure 1 Species-specific ACE2 usage of NeoCoV and several other ACE2-utilizing viruses.**
363 **a-b**, Most but not all ACE2 orthologs from Yin-bats were deficient in supporting NeoCoV and
364 PDF-2180 binding and entry. NeoCoV RBD-hFc binding (**a**) and pseudovirus entry efficiency (**b**)
365 were evaluated on HEK293T cells transiently expressing the indicated ACE2 orthologs. Vector
366 plasmid was used as a background control. Underline indicate species from Yang-bats. **c**, Distinct
367 RBD binding modes of four ACE2 utilizing coronaviruses. RBD footprints of SARS-CoV-2 (PDB:
368 6M0J, purple), NL63 (PDB: 3KBH, green), NeoCoV (PDB: 7WPO, blue) and PDF-2180 (PDB:
369 7WPZ, yellow) on indicated ACE2 were highlighted in red. **d,** Heat map of the RBD binding (mean
370 fluorescence value) and pseudovirus entry efficiency (RLU) of ACE2 utilizing coronaviruses on
371 HEK293T cells transiently expressing the indicated ACE2 orthologs. The pseudovirus entry
372 efficiency on hACE2 was set as 1.0 for SARS-CoV-2 and NL63. The efficiency on Lbor ACE2
373 (highest efficiency) was set as 1.0 for NeoCoV and PDF-2180. Mean±SD for **b** (n=3) ; Mean for **d**
374 (n=3). RLU: relative light units.

375

376 **Figure 2 Identification of host range determinants restricting NeoCoV/PDF-2180 recognition.**
377 **a,** The structure of NeoCoV RBD (purple) and Ppip ACE2 (rainbow) binding interface. Region 1 and
378 region 2 indicate two main interaction surfaces formed by two ACE2 loops with
379 glycosylations. **b-c,** Prediction of the potential host range determinants based on sequence
380 analysis. **b,** The sequence logo analyzes the residue conservation of sequences of the two critical
381 ACE2 loops based on 50 ACE2 functionally divided into two groups (**b**). Upper: efficiently support
382 entry. Lower, deficient in supporting entry. The pie charts show the numbers of Yin-bats and
383 Yang-bats in each group. **c,** Residues showing contrasting differences in frequency or contributing
384 critical interactions were defined as site A-D, and their location in full-length ACE2 was indicated
385 below. TM, transmembrane motif. **d,** Summary of defect types of bat and human ACE2 orthologs
386 according to their residue features in site A-D. The predicted sub-optional residues in site A (54-56),
387 B (305), C (329-330), and D (337-340) were highlighted with red, green, blue, and magenta,
388 respectively. *, sub-optional but acceptable by forming a hydrogen bond instead of salt
389 bridge. **e-i,** Structure modeling the impact of sub-optional residue substitution to the interaction
390 between Ppip ACE2 and NeoCoV RBD. **e,** Overall structure of Ppip ACE2 and NeoCoV RBD

complex, with each sites indicated by dashed boxes. **f-i,** Zoomed in structure details of the interactions in sites A-D in WT (upper) and mutated (lower) Ppip ACE2, respectively. All structures are shown as ribbon representations, with key residues rendered as sticks. Salt bridges and hydrogen bonds are shown as red and yellow dashed lines. Mutated residues were highlighted in purple.

Figure 3 Verification of determinants crucial for species-specific receptor usage in bats.

a-g, Effect of sites A-D gain-of-function mutants of Yin-bats' ACE2 orthologs on NeoCoV RBD and PDF-2180 RBD binding (**a, c, f**) and pseudovirus entry (**b, d, g**). **a-b,** Rsin ACE2 (defect type A); **c-d**, Rfer ACE2 (defect type B); **e-g,** Raeg ACE2 (defect type ABCD). **e,** Schematic illustration of Raeg ACE2 swap mutants with PpipACE2 counterparts. **h**, Flow cytometry analysis of NeoCoV and PDF-2180 RBD-hFc binding with HEK293T cells transiently expressing the indicated ACE2 orthologs. The vector is considered a negative control, and the Ppip ACE2 was employed as a positive control. The red dashed lines indicate the background to define the positive cells. **i**, BLI assays analyzing the binding kinetics between NeoCoV-RBD-hFc and PDF-2180-RBD-hFc and Raeg and Rsin ACE2 WT and mutated ectodomain proteins. Ppip ACE2 was used as a positive control. RLU: Relative luciferase unit. Mean±SD for **b, d, g.** n=3 for **b** and **d**, n=4 for **g**.

Figure 4. RBM mutation T510F enhances the cross-species transmission ability of NeoCoV in bats.

a, Structure showing NeoCoV-T510F interacting with a conserved hydrophobic pocket in Ppip ACE2. Residue conservation was indicated by red and blue colors. The side chains of hydrophobic residues that constitute the pocket were indicated as sticks. The blue and red color on the Ppip ACE2 shows the conservation ratio of 50 Bat ACE2 counterparts residues from low to high. **b,** The sequence logo of surrounding residues of the conserved hydrophobic pocket on 50 bat ACE2. The side chain hydrophobicity was shown in blew. **c-d,** NeoCoV RBD-T510F-hFc RBD binding (**c**) and pseudovirus entry (**d**) on HEK293T cells transiently expressing indicated bat ACE2 orthologs. **e.** The immunofluorescence analysis of the expression level of WT and mutated Raeg and Rsin ACE2. **f**. The NeoCoV-T510F pseudovirus entry to Raeg and Rsin ACE2 WT and mutants. RLU: relative light unit. Mean±SD for **d** and **f**, n=3.

421 **Extended data figure 1. The RBD binding efficiency of ACE2 utilizing CoVs in HEK293T cells**
422 **transiently expressing the indicated bats ACE2.**
423 **a,** The expression level of ACE2 orthologs examined by immunofluorescence assay detecting the C
424 terminal fused 3×Flag. **b-d,** The PDF-2180 (**b**), SARS-CoV-2 (**c**), and NL63 (**d**) RBD binding
425 (2μg/mL) on HEK293T cells transiently expressing the indicated bats ACE2.
426
427
428 **Extended data figure 2. The pseudovirus entry efficiency of ACE2 utilizing CoVs in HEK293T**
429 **cells transiently expressing the indicated bats ACE2.**
430 **a-c.** The entry efficiency of PDF-2180 (**a**), NL63 (**b**), and SARS-CoV-2 (**c**) pseudoviruses in
431 HEK293T cells transiently expressing the indicated bats ACE2. RLU: relative luciferase unit.
432
433 **Extended 3 Phylogenetic tree of the 50 bats ACE2 tested in this study.**
434 Phylogenetic tree was generated by the MEGA-X software based on the ACE2 protein sequences
435 from the 49 bats species (Two ACE2 sequences for Rsin) across the phylogeny**.** Yin-bats and
436 Yang-bats were highlighted by turquoise and coral backgrounds. The GenBank accession numbers
437 and protein sequences were summarized in supplementary table 1.
438
439 **Extended data figure 4. The multi-sequence alignments of 50 bats ACE2.**
440 The sequence alignment was conducted based on sequences around sites A, B, C, and site D by the
441 Clustal W. Identical residues were highlighted in red, and similar residues were in the blue frames.
442
443 **Extended data figure 5. Western blot analysis of the Rsin, Rfer, and Raeg ACE2 expression**
444 **levels.**
445 **a-c.** Western blot analysis of the WT and mutant Rsin(**a**), Rfer(**b**), and Raeg(**c**) ACE2 expression
446 levels in HEK293T cells detecting the C-terminal fused 3×Flag tag. Mw: molecular weight.
447
448 **Extended data figure 6. Verification of mutants on Nlep, Hgal, Rpea, and Rmal ACE2 with**
449 **improved NeoCoV/PDF-2180 RBD binding and PSV entry efficiency.**

a, Expression levels of the WT and mutated Rpea and Rmal ACE2 by immunofluorescence. **b,** The NeoCoV and PDF-2180 PSV entry efficiency supported by WT and mutated Rpea and Rmal ACE2 in HEK293T cells. **c,** NeoCoV or PDF-2180 RBD binding efficiency on HEK293T cells expressing the WT Hgal ACE2 and related mutants. **d,** The NeoCoV, and PDF-2180 PSV entry efficiency into the HEK293T cells transiently expressing WT and mutated Hgal ACE2. **e,** Western blot analysis of the WT and mutated Hgal ACE2 expression in HEK293T cells.**f,** Schematic illustration of Nlep ACE2 swap mutants with PpipACE2 counterparts. **g,** The binding efficiency of NeoCoV and PDF-2180 RBD to the WT and mutated Nlep ACE2. **h,** Entry efficiency of NeoCoV and PDF-2180 spike pseudotyped virus into the Nlep ACE2 mutants transiently expressing on the HEK293T cells. **i,** Western blot analysis of the Nlep ACE2 mutants expression levels in HEK293T cells. RLU: relative luciferase unit. Mean±SD for **c**, **f**, **i** (n=3). Mw: molecular weight.

Extended data figure 7 NeoCoV and PDF-2180 pseudotyped virus entry in Tb1 Lu cells transiently expressing WT and mutated Raeg and Rsin ACE2.

a. ACE2 expression level of WT and mutated Raeg and Rsin ACE2 in HEK293T cells by detecting the C terminal fused 3×Flag tag by immunofluorescence. **b-d,** NeoCoV and PDF-2180 pseudoviruses entry efficiency at 16 h post-infection were indicated by (GFP) (**b**) and luciferase activity (**c-d**).

1 Li, F. Receptor recognition mechanisms of coronaviruses: a decade of structural studies. *J Virol* **89**, 1954-1964, doi:10.1128/JVI.02615-14 (2015).

2 Xiong, Q. *et al. bioRxiv*, doi:10.1101/2022.01.24.477490 (2022).

3 Chen, L. *et al.* RNA based mNGS approach identifies a novel human coronavirus from two individual pneumonia cases in 2019 Wuhan outbreak. *Emerg Microbes Infect* **9**, 313-319, doi:10.1080/22221751.2020.1725399 (2020).

4 Ksiazek, T. G. *et al.* A novel coronavirus associated with severe acute respiratory syndrome. *N Engl J Med* **348**, 1953-1966, doi:10.1056/NEJMoa030781 (2003).

5 Zaki, A. M., van Boheemen, S., Bestebroer, T. M., Osterhaus, A. D. & Fouchier, R. A. Isolation of a novel coronavirus from a man with pneumonia in Saudi Arabia. *N Engl J Med* **367**, 1814-1820, doi:10.1056/NEJMoa1211721 (2012).

483 6 Zhou, P. *et al.* A pneumonia outbreak associated with a new coronavirus of probable bat origin. *Nature*
484 **579**, 270-273, doi:10.1038/s41586-020-2012-7 (2020).
485 7 Ge, X. Y. *et al.* Isolation and characterization of a bat SARS-like coronavirus that uses the ACE2 receptor.
486 *Nature* **503**, 535-538, doi:10.1038/nature12711 (2013).
487 8 Latinne, A. *et al.* Origin and cross-species transmission of bat coronaviruses in China. *Nat Commun* **11**,
488 4235, doi:10.1038/s41467-020-17687-3 (2020).
489 9 Temmam, S. *et al.* Bat coronaviruses related to SARS-CoV-2 and infectious for human cells. *Nature* **604**,
490 330-336, doi:10.1038/s41586-022-04532-4 (2022).
491 10 Wang, Q. *et al.* Bat origins of MERS-CoV supported by bat coronavirus HKU4 usage of human receptor
492 CD26. *Cell Host Microbe* **16**, 328-337, doi:10.1016/j.chom.2014.08.009 (2014).
493 11 Wong, A. C. P., Li, X., Lau, S. K. P. & Woo, P. C. Y. Global Epidemiology of Bat Coronaviruses. *Viruses* **11**,
494 doi:10.3390/v11020174 (2019).
495 12 Memish, Z. A. *et al.* Middle East respiratory syndrome coronavirus in bats, Saudi Arabia. *Emerg Infect Dis*
496 **19**, 1819-1823, doi:10.3201/eid1911.131172 (2013).
497 13 Zhang, Z., Shen, L. & Gu, X. Evolutionary Dynamics of MERS-CoV: Potential Recombination, Positive
498 Selection and Transmission. *Sci Rep* **6**, 25049, doi:10.1038/srep25049 (2016).
499 14 Mohd, H. A., Al-Tawfiq, J. A. & Memish, Z. A. Middle East Respiratory Syndrome Coronavirus (MERS-CoV)
500 origin and animal reservoir. *Virol J* **13**, 87, doi:10.1186/s12985-016-0544-0 (2016).
501 15 Anthony, S. J. *et al.* Further Evidence for Bats as the Evolutionary Source of Middle East Respiratory
502 Syndrome Coronavirus. *mBio* **8**, doi:10.1128/mBio.00373-17 (2017).
503 16 Corman, V. M. *et al.* Rooting the phylogenetic tree of middle East respiratory syndrome coronavirus by
504 characterization of a conspecific virus from an African bat. *J Virol* **88**, 11297-11303,
505 doi:10.1128/JVI.01498-14 (2014).
506 17 Geldenhuys, M. *et al.* A metagenomic viral discovery approach identifies potential zoonotic and novel
507 mammalian viruses in Neoromicia bats within South Africa. *PLoS One* **13**, e0194527,
508 doi:10.1371/journal.pone.0194527 (2018).
509 18 Corman, V. M. *et al.* Characterization of a novel betacoronavirus related to middle East respiratory
510 syndrome coronavirus in European hedgehogs. *J Virol* **88**, 717-724, doi:10.1128/JVI.01600-13 (2014).
511 19 Ithete, N. L. *et al.* Close relative of human Middle East respiratory syndrome coronavirus in bat, South
512 Africa. *Emerg Infect Dis* **19**, 1697-1699, doi:10.3201/eid1910.130946 (2013).
513 20 Lau, S. K. P. *et al.* Identification of a Novel Betacoronavirus (Merbecovirus) in Amur Hedgehogs from China.
514 *Viruses* **11**, doi:10.3390/v11110980 (2019).
515 21 Yan, H. *et al.* ACE2 receptor usage reveals variation in susceptibility to SARS-CoV and SARS-CoV-2
516 infection among bat species. *Nat Ecol Evol* **5**, 600-608, doi:10.1038/s41559-021-01407-1 (2021).
517 22 Huynh, J. *et al.* Evidence supporting a zoonotic origin of human coronavirus strain NL63. *J Virol* **86**,
518 12816-12825, doi:10.1128/JVI.00906-12 (2012).
519 23 Wilson, D. E. M., R. A. Handbook of the Mammals of the World. **Vol. 9: Bats (Lynx, 2019)** (2019).
520 24 King, S. B. & Singh, M. Comparative genomic analysis reveals varying levels of mammalian adaptation to
521 coronavirus infections. *PLoS Comput Biol* **17**, e1009560, doi:10.1371/journal.pcbi.1009560 (2021).
522 25 Liu, Y. *et al.* Functional and genetic analysis of viral receptor ACE2 orthologs reveals a broad potential host
523 range of SARS-CoV-2. *Proc Natl Acad Sci U S A* **118**, doi:10.1073/pnas.2025373118 (2021).
524 26 Letko, M. *et al.* Adaptive Evolution of MERS-CoV to Species Variation in DPP4. *Cell Rep* **24**, 1730-1737,
525 doi:10.1016/j.celrep.2018.07.045 (2018).
526 27 Hu, B. *et al.* Discovery of a rich gene pool of bat SARS-related coronaviruses provides new insights into

527 the origin of SARS coronavirus. *PLoS Pathog* **13**, e1006698, doi:10.1371/journal.ppat.1006698 (2017).
528 28 Mehdipour, A. R. & Hummer, G. Dual nature of human ACE2 glycosylation in binding to SARS-CoV-2
529 spike. *Proc Natl Acad Sci U S A* **118**, doi:10.1073/pnas.2100425118 (2021).
530 29 Tortorici, M. A. *et al.* Structure, receptor recognition, and antigenicity of the human coronavirus
531 CCoV-HuPn-2018 spike glycoprotein. *Cell* **185**, 2279-2291 e2217, doi:10.1016/j.cell.2022.05.019 (2022).
532 30 Zhang, Y. *et al.* Cross-species tropism and antigenic landscapes of circulating SARS-CoV-2 variants. *Cell*
533 *Rep* **38**, 110558, doi:10.1016/j.celrep.2022.110558 (2022).
534 31 Letunic, I. & Bork, P. Interactive Tree Of Life (iTOL) v5: an online tool for phylogenetic tree display and
535 annotation. *Nucleic Acids Res* **49**, W293-W296, doi:10.1093/nar/gkab301 (2021).
536 32 Pettersen, E. F. *et al.* UCSF ChimeraX: Structure visualization for researchers, educators, and developers.
537 *Protein Sci* **30**, 70-82, doi:10.1002/pro.3943 (2021).
538 33 Whitt, M. A. Generation of VSV pseudotypes using recombinant DeltaG-VSV for studies on virus entry,
539 identification of entry inhibitors, and immune responses to vaccines. *J Virol Methods* **169**, 365-374,
540 doi:10.1016/j.jviromet.2010.08.006 (2010).
541 34 Biacchesi, S. *et al.* Rapid human metapneumovirus microneutralization assay based on green fluorescent
542 protein expression. *J Virol Methods* **128**, 192-197, doi:10.1016/j.jviromet.2005.05.005 (2005).
543 35 Nie, J. *et al.* Quantification of SARS-CoV-2 neutralizing antibody by a pseudotyped virus-based assay. *Nat*
544 *Protoc* **15**, 3699-3715, doi:10.1038/s41596-020-0394-5 (2020).

545

Figure1

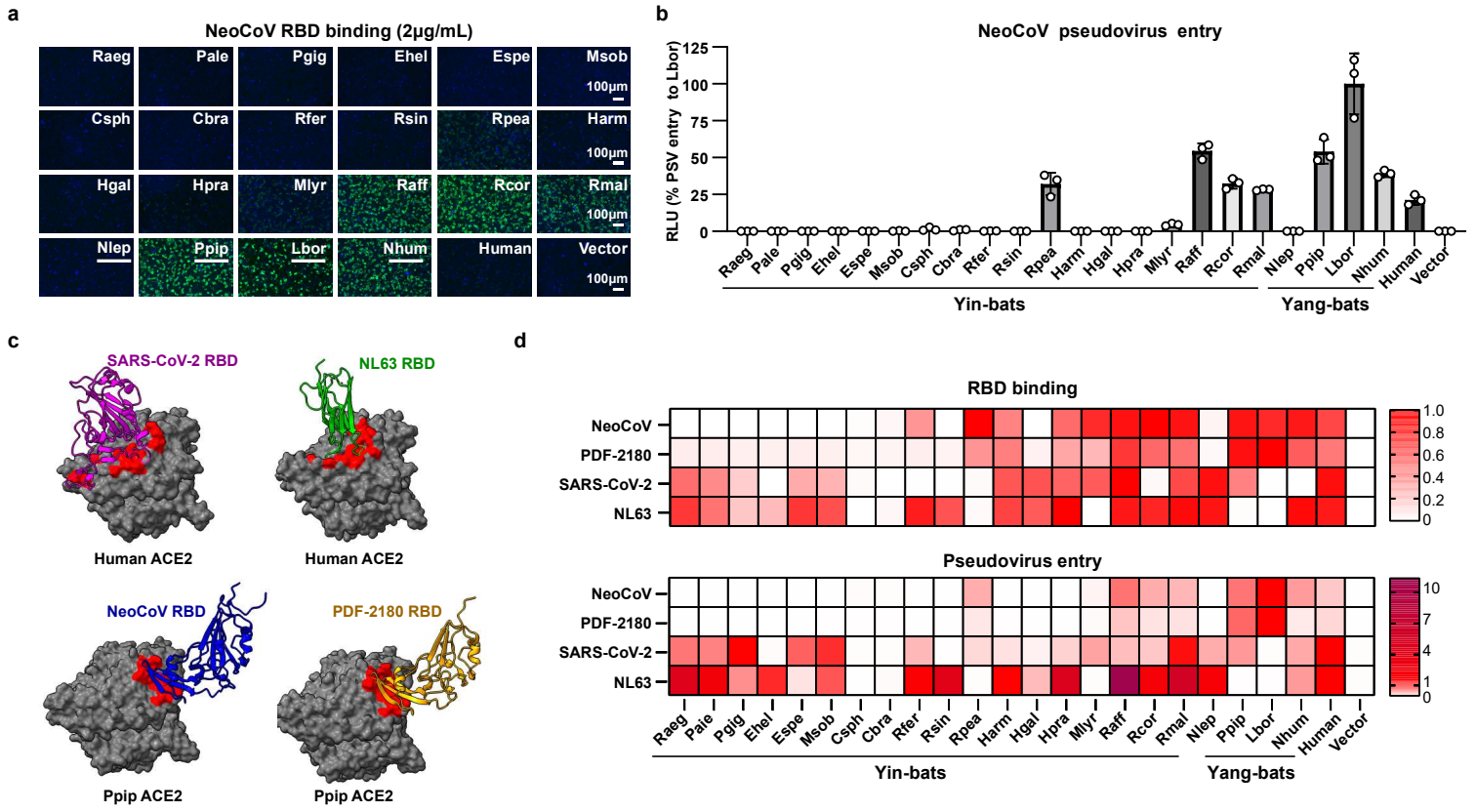
a
NeoCoV RBD binding (2μg/mL)
Raeg
Pale
Pgig
Ehel
Espe
Msob
Csph
Cbra
Rfer
Rsin
Rpea
Harm
Hgal
Hpra
Mlyr
Raff
Rcor
Rmal
Nlep
Ppip
Lbor
Nhum
Human
Vector
100μm
b
NeoCoV pseudovirus entry
RLU (% PSV entry to Lbor)
125
100
75
50
25
0
Yin-bats
Yang-bats
c
SARS-CoV-2 RBD
NL63 RBD
Human ACE2
Human ACE2
NeoCoV RBD
PDF-2180 RBD
Ppip ACE2
Ppip ACE2
d
RBD binding
NeoCoV
PDF-2180
SARS-CoV-2
NL63
1.0
0.8
0.6
0.4
0.2
0
Pseudovirus entry
10
7
4
1
0
Yin-bats
Yang-bats

Figure2

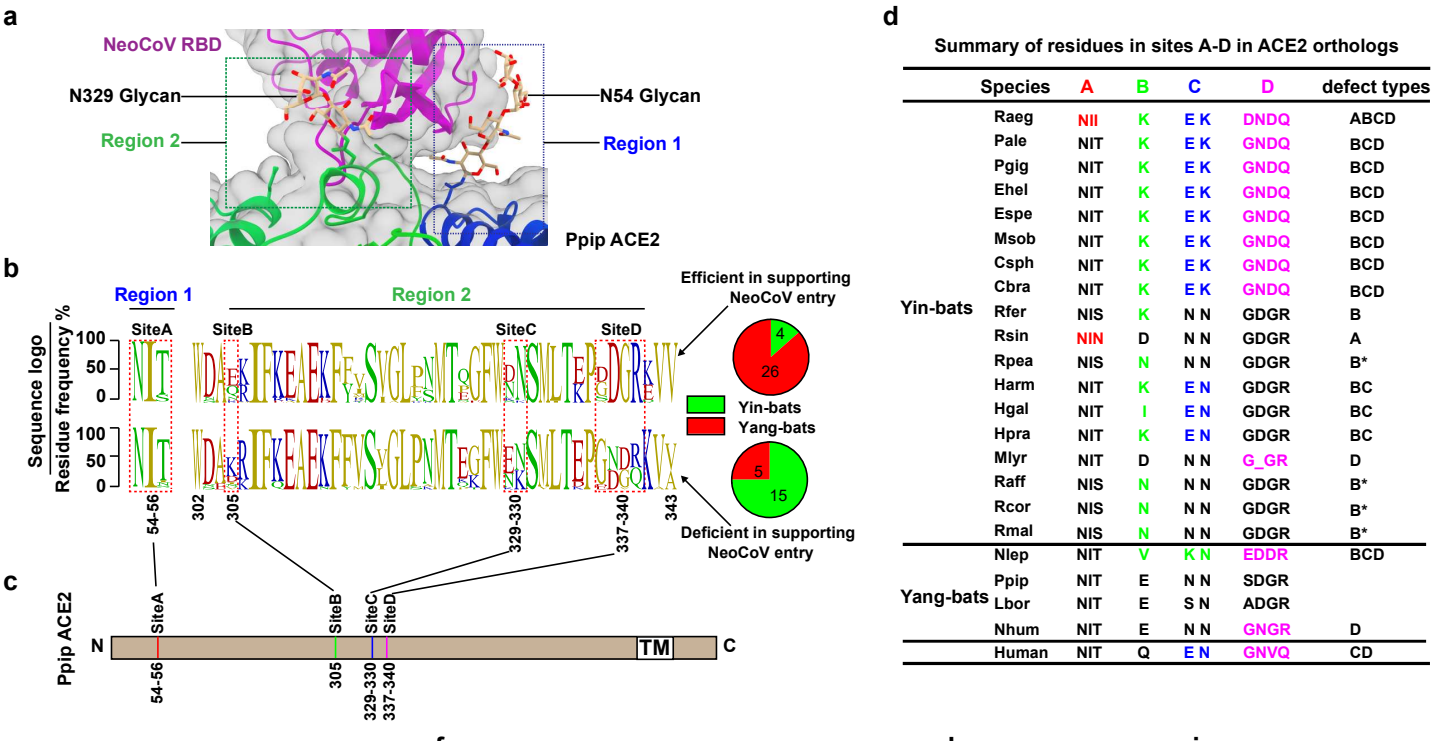

	Species	A	B	C	D	defect types
Yin-bats	Raeg	NII	K	E K	DNDQ	ABCD
	Pale	NIT	K	E K	GNDQ	BCD
	Pgig	NIT	K	E K	GNDQ	BCD
	Ehel	NIT	K	E K	GNDQ	BCD
	Espe	NIT	K	E K	GNDQ	BCD
	Msob	NIT	K	E K	GNDQ	BCD
	Csph	NIT	K	E K	GNDQ	BCD
	Cbra	NIT	K	E K	GNDQ	BCD
	Rfer	NIS	K	N N	GDGR	B
	Rsin	NIN	D	N N	GDGR	A
	Rpea	NIS	N	N N	GDGR	B*
	Harm	NIT	K	E N	GDGR	BC
	Hgal	NIT	I	E N	GDGR	BC
	Hpra	NIT	K	E N	GDGR	BC
	Mlyr	NIT	D	N N	G_GR	D
	Raff	NIS	N	N N	GDGR	B*
	Rcor	NIS	N	N N	GDGR	B*
	Rmal	NIS	N	N N	GDGR	B*
Yang-bats	Nlep	NIT	V	K N	EDDR	BCD
	Ppip	NIT	E	N N	SDGR	
	Lbor	NIT	E	S N	ADGR	
	Nhum	NIT	E	N N	GNGR	D
	Human	NIT	Q	E N	GNVQ	CD

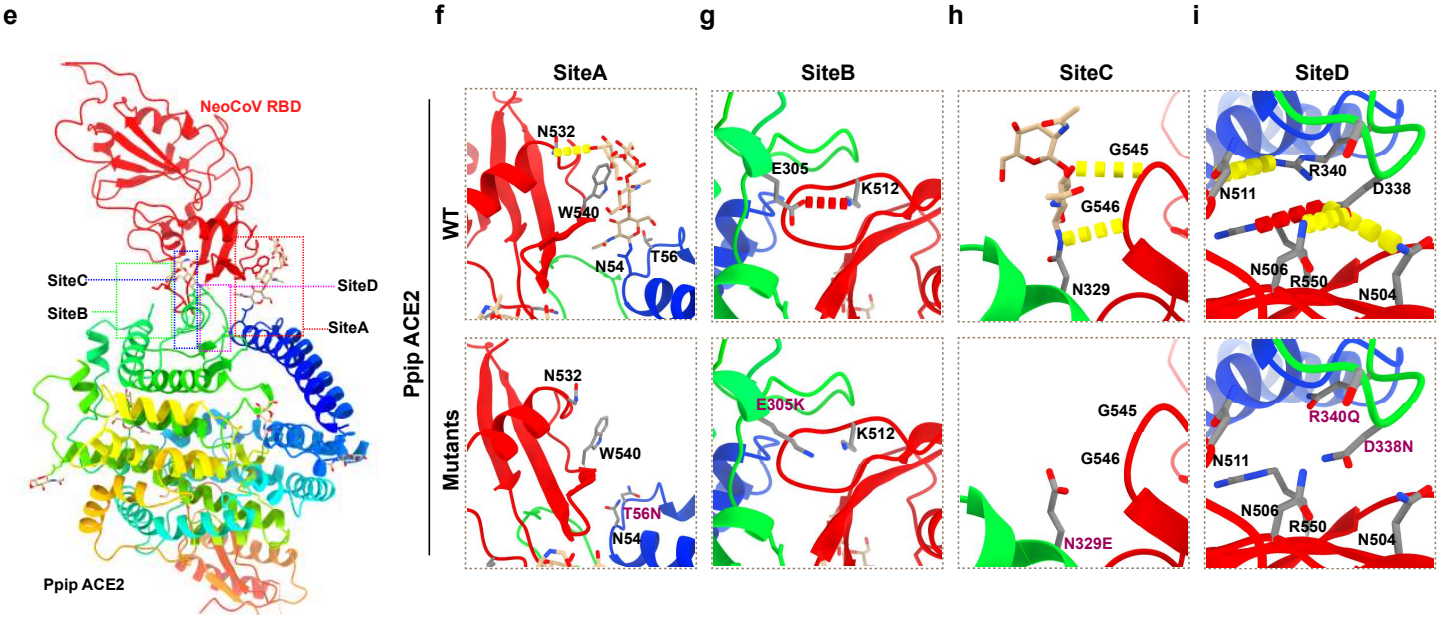

Figure3

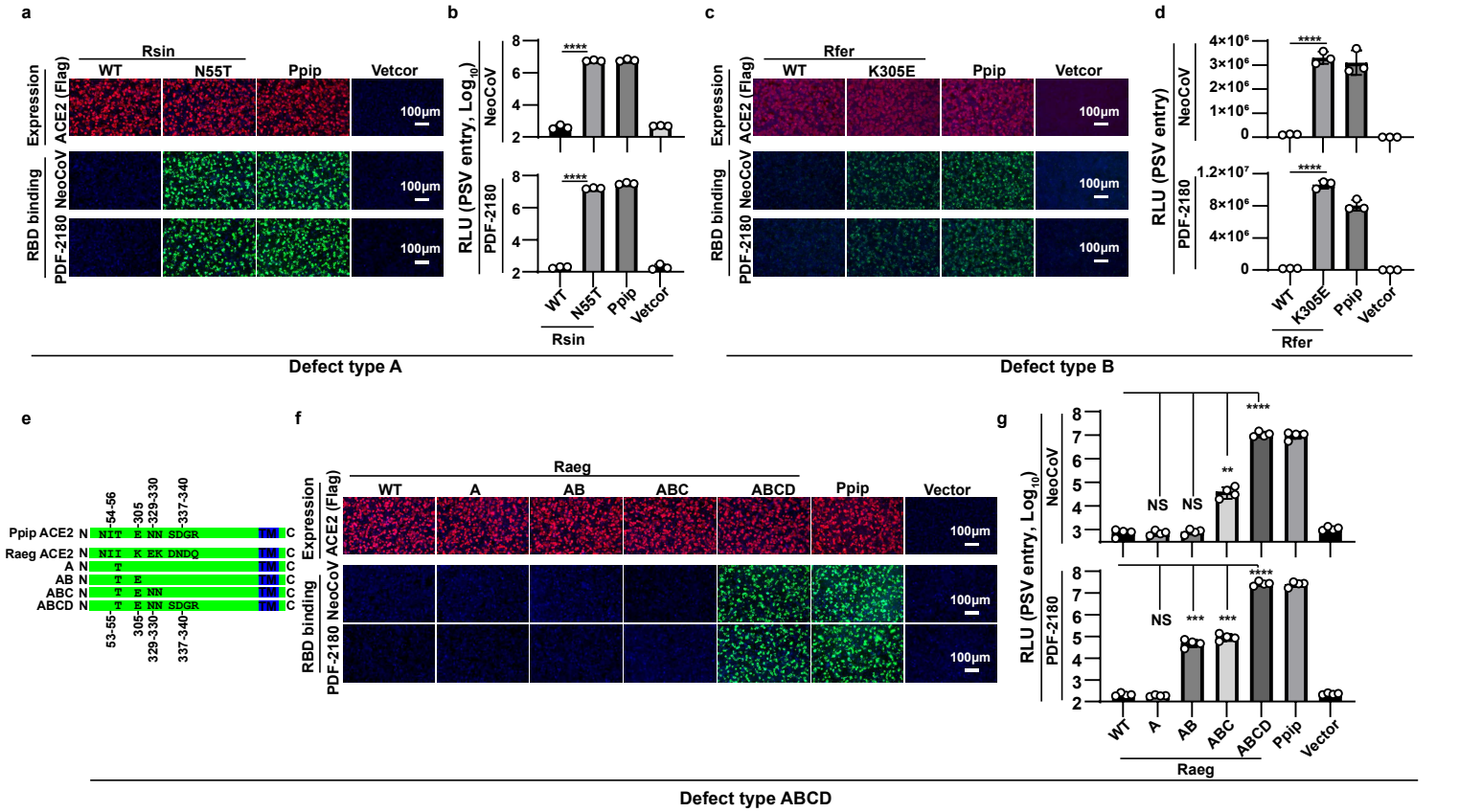
a
Rsin
WT
N55T
Ppip
Vetcor
Expression
ACE2 (Flag)
RBD binding
NeoCoV
PDF-2180
100μm
b
RLU (PSV entry, Log10)
NeoCoV
PDF-2180
****
WT
N55T
Ppip
Vetcor
Rsin
c
Rfer
WT
K305E
Ppip
Vetcor
d
RLU (PSV entry)
K305E
Rfer
Defect type A
Defect type B
e
Ppip ACE2 N
Raeg ACE2 N
A N
AB N
ABC N
ABCD N
54-56
305
329-330
337-340
53-55
f
Raeg
WT
A
AB
ABC
ABCD
Ppip
Vector
g
NS
**
***
Defect type ABCD
h
NeoCoV
PDF-2180
0.11±0.03%
1.43±0.18%
Vector
87.9±0.5%
73.95±0.35%
Ppip ACE2
0.15±0.02%
0.73±0.1%
Rsin ACE2
87.7±0.02%
63.6±0.4%
Rsin ACE2 (N55T)
0.23±0.08%
1.75±0.2%
Raeg ACE2
86.15±0.55%
59.25±0.55%
Raeg ACE2 (ABCD)
Cell counts
RBD binding
i
500nM
250nM
125nM
62.5nM
31.25nM
15.625nM
Raeg ACE2 WT
Raeg ACE2 (ABCD)
Rsin ACE2 WT
Rsin ACE2 N55T
Ppip ACE2
NeoCoV RBD
PDF-2180 RBD
Response(nm)
Time(s)
KD(M)=2.35E-08
kon(Ms-1)=5.88E+03
koff(S-1)=1.38E-04
R2=0.9978
KD(M)=2.04E-08
kon(Ms-1)=3.99E+04
koff(S-1)=8.12E-04
R2=0.9978
KD(M)=1.78E-09
kon(Ms-1)=5.85E+04
koff(S-1)=1.04E-04
R2=0.9981
KD(M)=6.94E-10
kon(Ms-1)=1.58E+04
koff(S-1)=1.10E-05
R2=0.9987
SSG KD(M)=6.94E-10
SSG R2=0.9987
KD(M)=4.17E-10
kon(Ms-1)=1.33E+05
koff(S-1)=5.54E-05
R2=0.9920

Figure 4

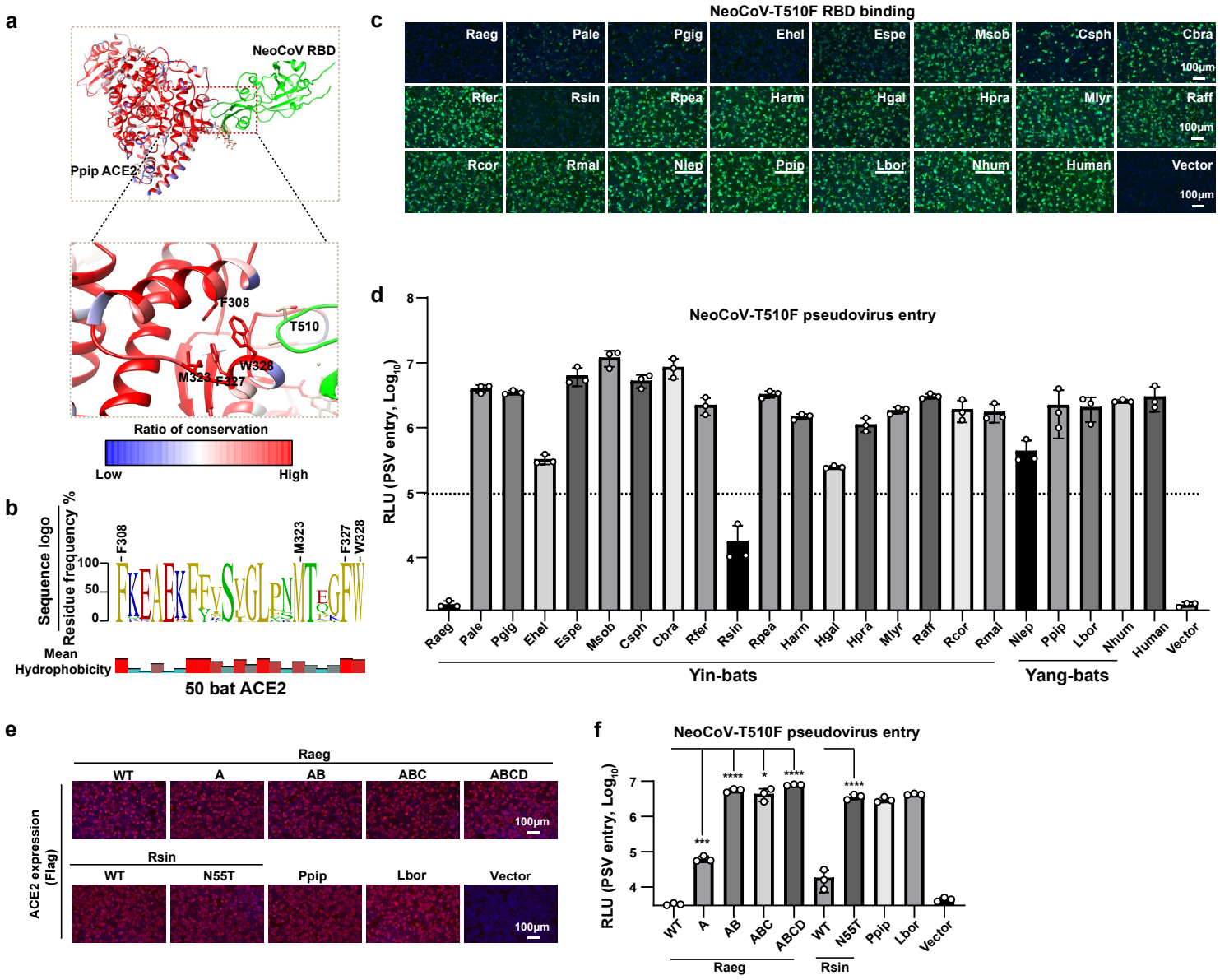
a
NeoCoV RBD
Ppip ACE2
F308
T510
W328
M323
F327
Ratio of conservation
Low
High
b
Sequence logo
Residue frequency %
F308
M323
F327
W328
Mean Hydrophobicity
50 bat ACE2
c
NeoCoV-T510F RBD binding
Raeg
Pale
Pgig
Ehel
Espe
Msob
Csph
Cbra
Rfer
Rsin
Rpea
Harm
Hgal
Hpra
Mlyr
Raff
Rcor
Rmal
Nlep
Ppip
Lbor
Nhum
Human
Vector
100μm
d
NeoCoV-T510F pseudovirus entry
RLU (PSV entry, Log10)
Yin-bats
Yang-bats
e
Raeg
WT
A
AB
ABC
ABCD
Rsin
N55T
Ppip
Lbor
Vector
ACE2 expression (Flag)
100μm
f
NeoCoV-T510F pseudovirus entry
RLU (PSV entry, Log10)
Raeg
Rsin

Extended 1

a

ACE2 expression-HEK293T cells

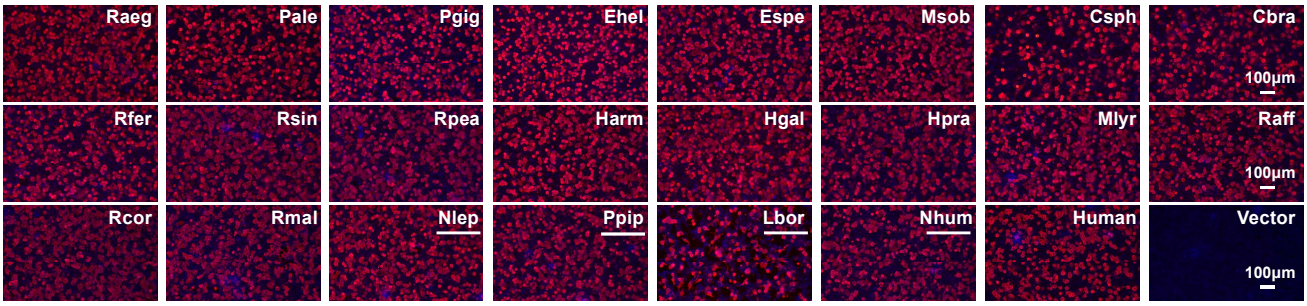

b

PDF-2180 RBD binding

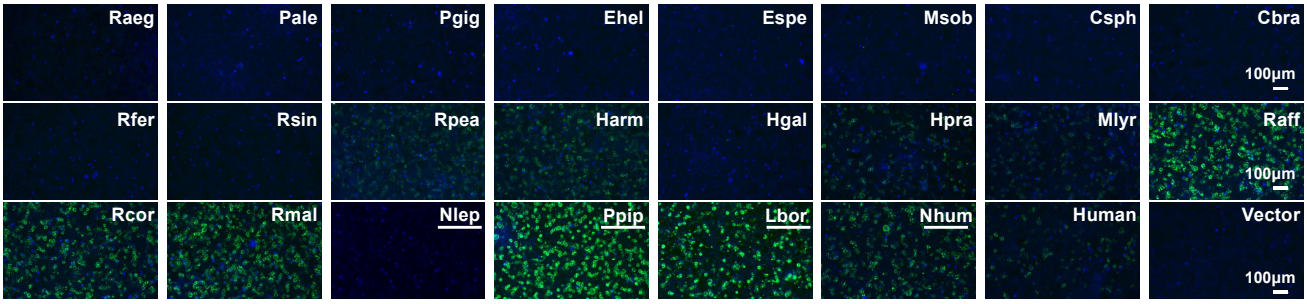

c

SARS-CoV-2 RBD binding

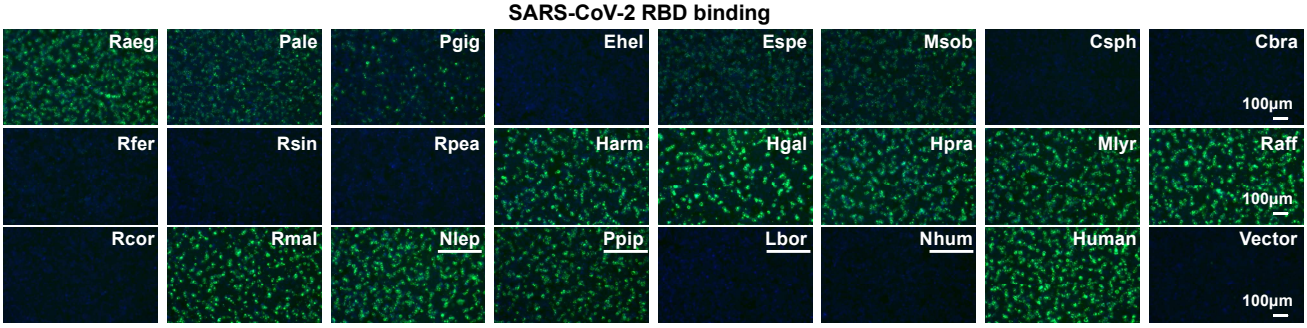

d

NL63 RBD binding

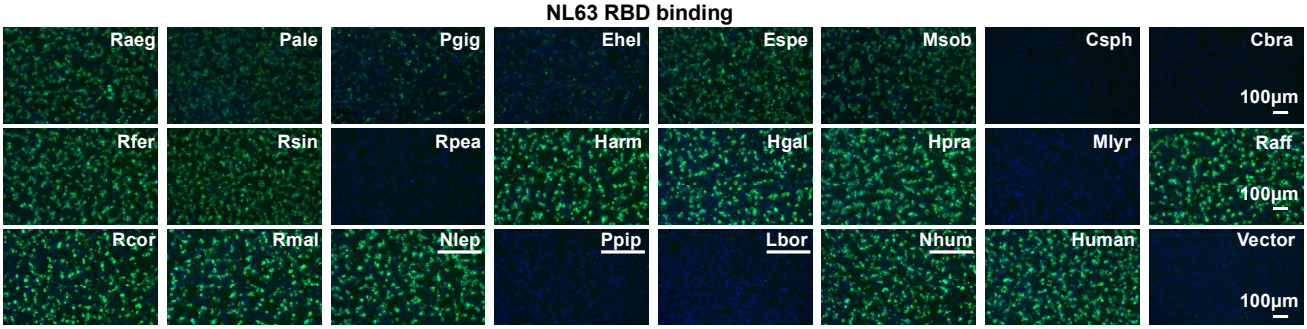

Extended 2

a

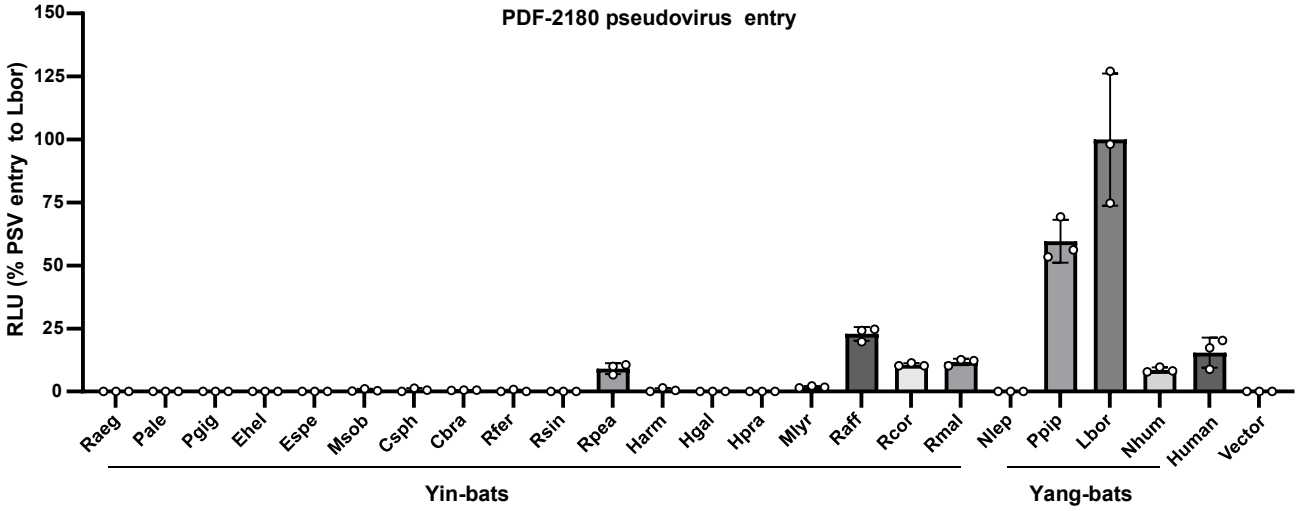

b

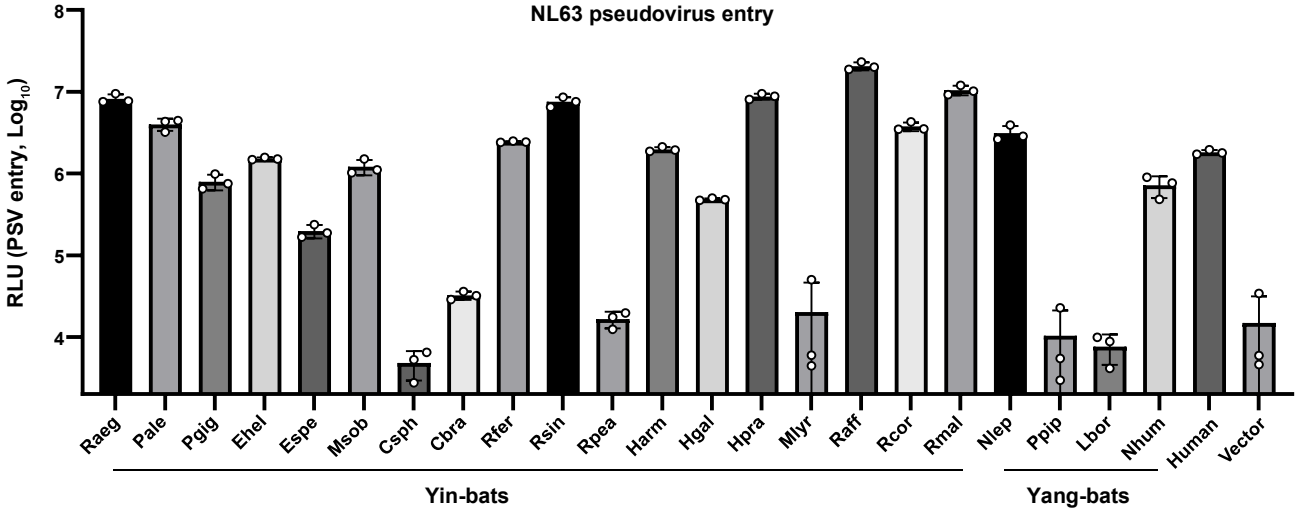

c

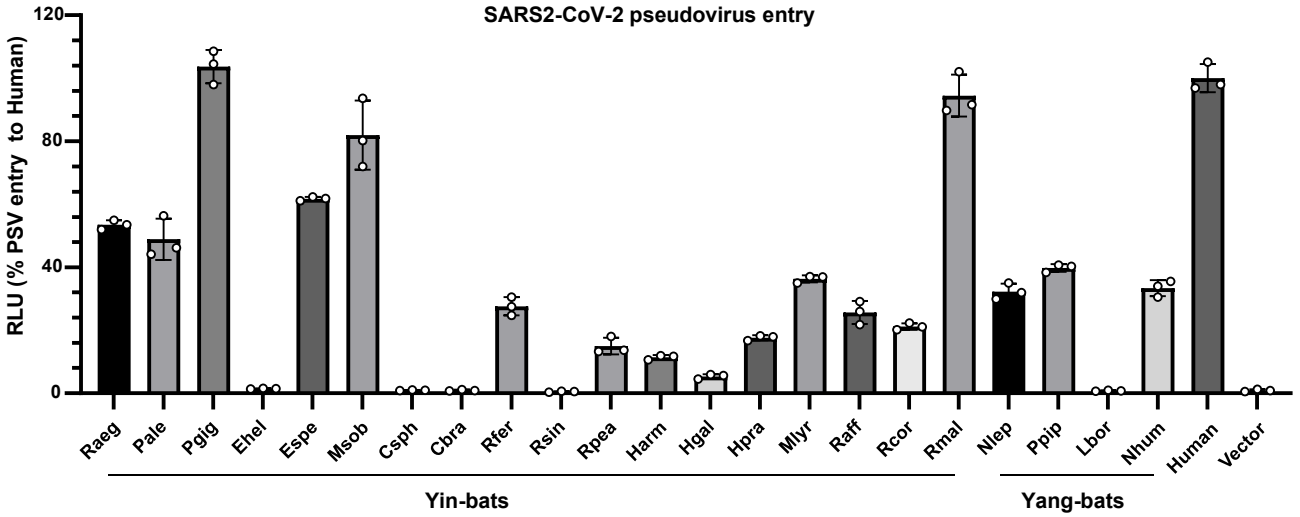

Extended 3

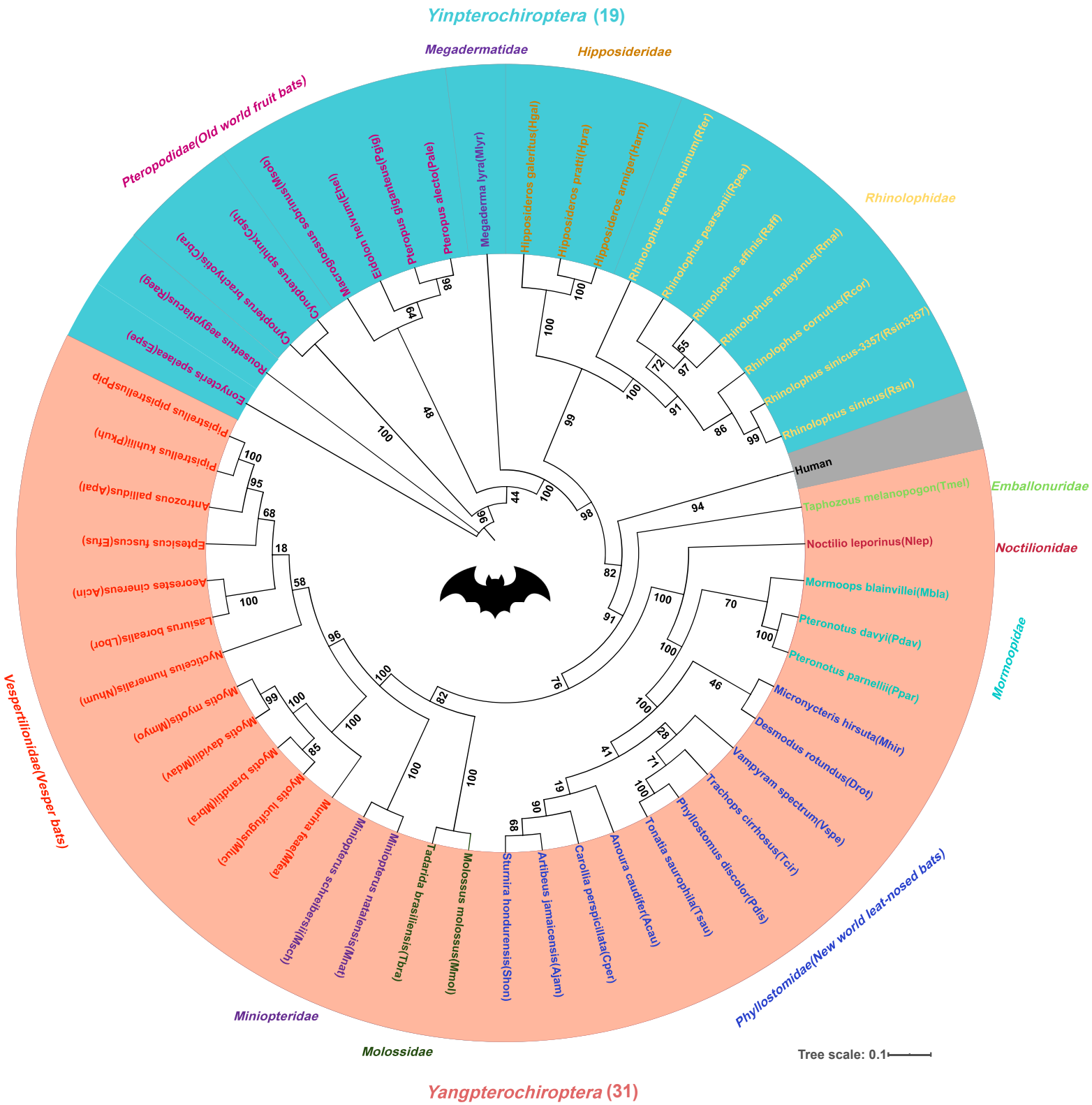
Yinpterochiroptera (19)
Megadermatidae
Hipposideridae
Pteropodidae(Old world fruit bats)
Rhinolophidae
Megaderma lyra(Mlyr)
Hipposideros galeritus(Hgal)
Hipposideros pratti(Hpra)
Hipposideros armiger(Harm)
Rhinolophus ferrumequinum(Rfer)
Rhinolophus pearsonii(Rpea)
Rhinolophus affinis(Raff)
Rhinolophus malayanus(Rmal)
Rhinolophus cornutus(Rcor)
Rhinolophus sinicus-3357(Rsin3357)
Rhinolophus sinicus(Rsin)
Pteropus alecto(Pale)
Pteropus gigantesus(Pgig)
Eidolon helvum(Ehel)
Macroglossus sobrinus(Msob)
Cynopterus sphinx(Csph)
Cynopterus brachyotis(Cbra)
Rousettus aegyptiacus(Raeg)
Eonycteris spelaea(Espe)
Human
Emballonuridae
Taphozous melanopogon(Tmel)
Noctilionidae
Noctilio leporinus(Nlep)
Mormoopidae
Mormoops blainvillei(Mbla)
Pteronotus davyi(Pdav)
Pteronotus parnellii(Ppar)
Micronycteris hirsuta(Mhir)
Desmodus rotundus(Drot)
Vampyram spectrum(Vspe)
Trachops cirrhosus(Tcir)
Phyllostomus discolor(Pdis)
Tonatia saurophila(Tsau)
Anoura caudifer(Acau)
Carollia perspicillata(Cper)
Artibeus jamaicensis(Ajam)
Sturnira hondurensis(Shon)
Molossus molossus(Mmol)
Tadarida brasiliensis(Tbra)
Miniopterus nataliensis(Mnat)
Miniopterus schreibersii(Msch)
Murina feae(Mfea)
Myotis lucifugus(Mluc)
Myotis brandtii(Mbra)
Myotis davidii(Mdav)
Myotis myotis(Mmyo)
Nycticeius humeralis(Nhum)
Lasiurus borealis(Lbor)
Aeorestes cinereus(Acin)
Eptesicus fuscus(Efus)
Antrozous pallidus(Apal)
Pipistrellus kuhlii(Pkuh)
Pipistrellus pipistrellus(Ppip)
Vespertilionidae(Vesper bats)
Miniopteridae
Molossidae
Phyllostomidae(New world leat-nosed bats)
Tree scale: 0.1
Yangpterochiroptera (31)

Extended 4

| | Site A | | | Site B | | |

Extended 5

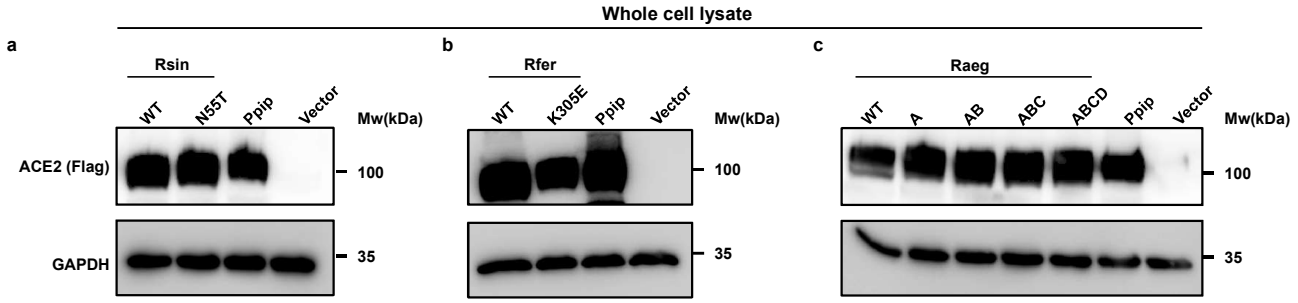
Whole cell lysate
a
Rsin
WT
N55T
Ppip
Vector
Mw(kDa)
ACE2 (Flag)
100
GAPDH
35
b
Rfer
WT
K305E
Ppip
Vector
Mw(kDa)
100
35
c
Raeg
WT
A
AB
ABC
ABCD
Ppip
Vector
Mw(kDa)
100
35

Extended 6

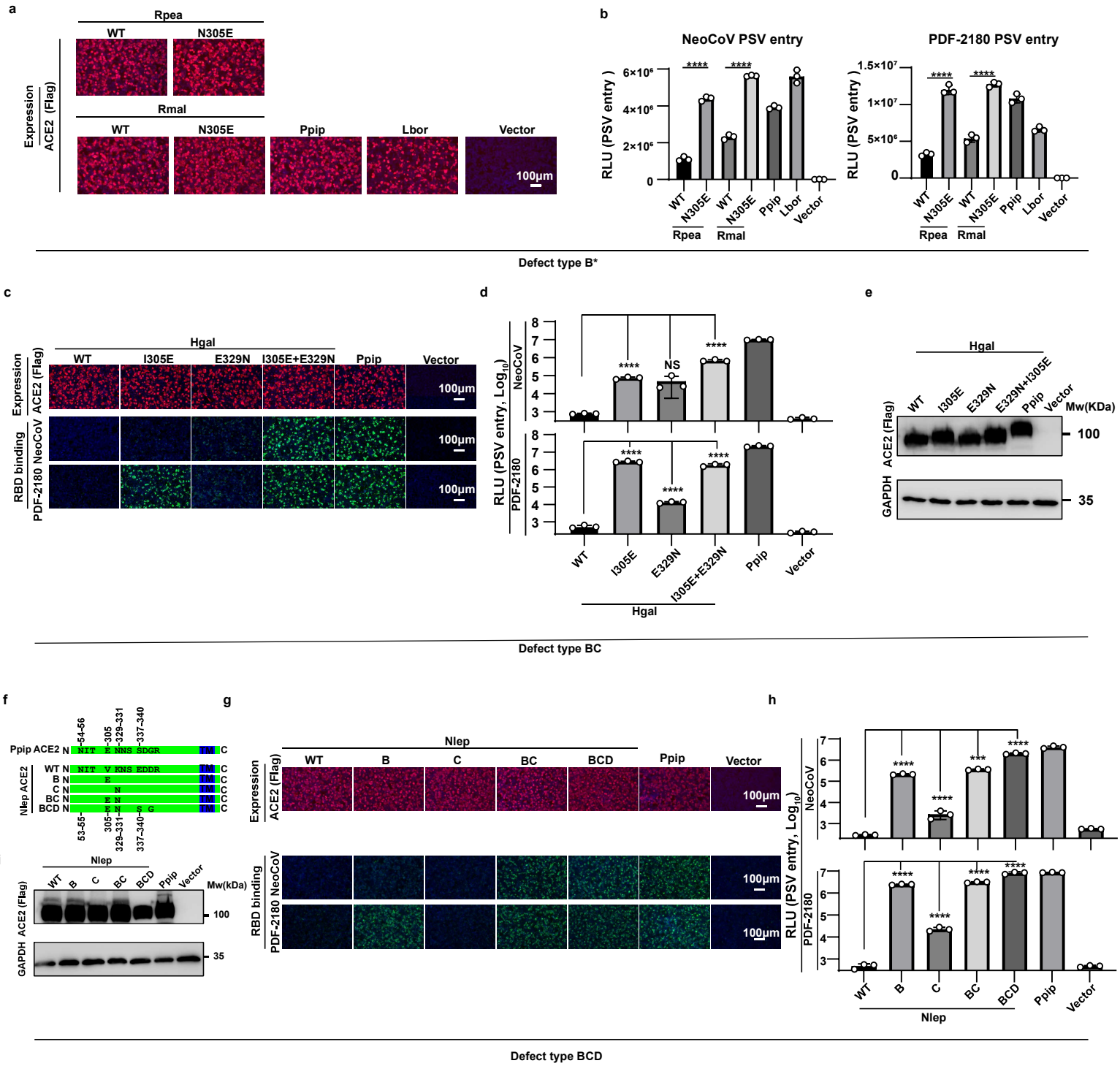
a
Rpea
WT
N305E
Rmal
WT
N305E
Ppip
Lbor
Vector
Expression
ACE2 (Flag)
100μm
b
NeoCoV PSV entry
PDF-2180 PSV entry
RLU (PSV entry)
WT
N305E
Ppip
Lbor
Vector
Rpea
Rmal
Defect type B*
c
Hgal
WT
I305E
E329N
I305E+E329N
Ppip
Vector
Expression
ACE2 (Flag)
RBD binding
NeoCoV
PDF-2180
100μm
d
RLU (PSV entry, Log10)
NeoCoV
PDF-2180
NS
WT
I305E
E329N
I305E+E329N
Ppip
Vector
Hgal
e
Hgal
WT
I305E
E329N
E329N+I305E
Ppip
Vector
Mw(KDa)
ACE2 (Flag)
GAPDH
100
35
Defect type BC
f
Ppip ACE2
WT
B
C
BC
BCD
Nlep ACE2
54-56
305
329-331
337-340
53-55
g
Nlep
WT
B
C
BC
BCD
Ppip
Vector
Expression
ACE2 (Flag)
RBD binding
NeoCoV
PDF-2180
100μm
h
RLU (PSV entry, Log10)
NeoCoV
PDF-2180
Nlep
i
Nlep
Mw(kDa)
ACE2 (Flag)
GAPDH
100
35
Defect type BCD

Extended 7

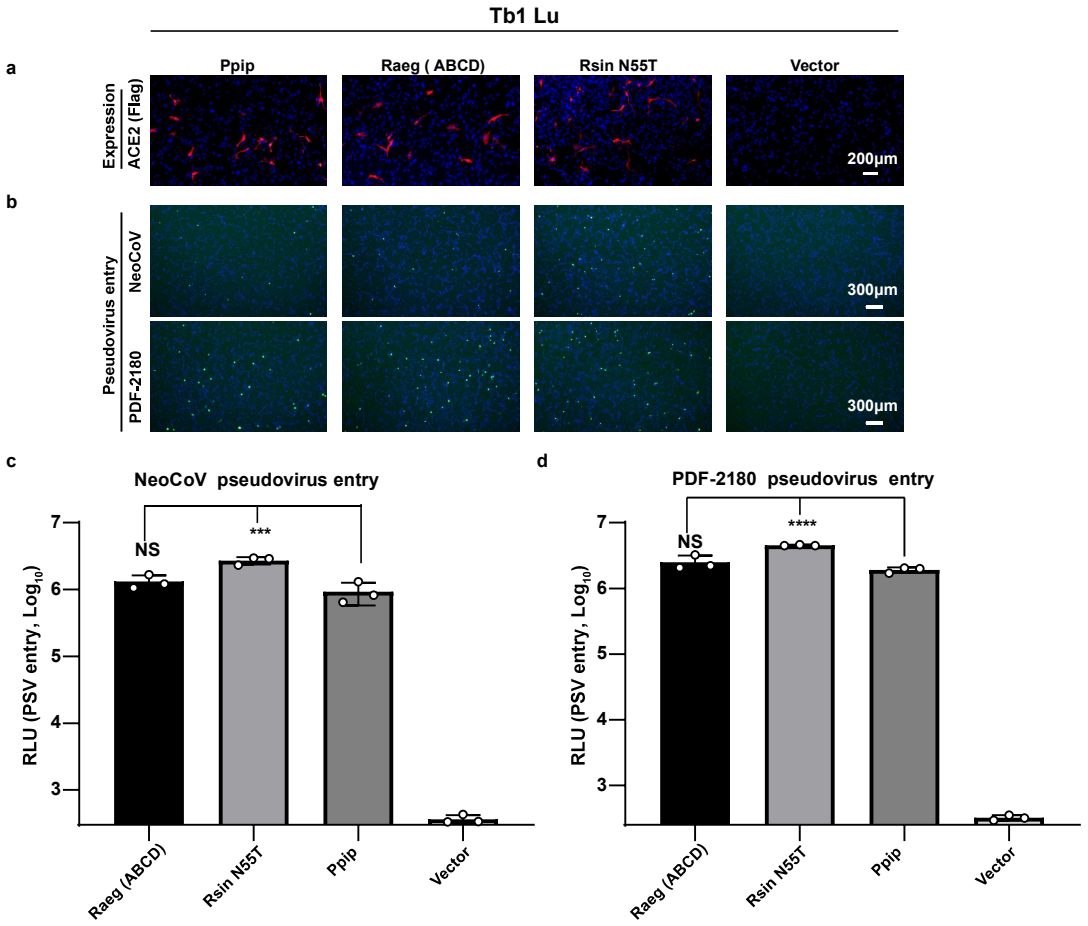
Tb1 Lu
a
Ppip
Raeg (ABCD)
Rsin N55T
Vector
Expression
ACE2 (Flag)
200μm
b
Pseudovirus entry
NeoCoV
PDF-2180
300μm
300μm
c
NeoCoV pseudovirus entry
RLU (PSV entry, Log10)
NS
***
Raeg (ABCD)
Rsin N55T
Ppip
Vector
d
PDF-2180 pseudovirus entry
RLU (PSV entry, Log10)
NS
****
Raeg (ABCD)
Rsin N55T
Ppip
Vector